An Analysis of Mixing in a Typical Experimental Setup to Measure Nucleation Rates of Precipitation Processes

By *Mark Roelands**, *Jos Derksen*, *Joop ter Horst*, *Herman Kramer*, and *Peter Jansens*

Mixing in a typical experimental setup to measure nucleation rates in precipitation processes was assessed. To determine these rates as a function of the driving force for concomitant polymorphs, it is necessary to perform these experiments at constant supersaturation. Therefore, the mixing time must be shorter than the time for the first nuclei to appear. For fast precipitation processes complete mixing has to be achieved within milliseconds. The mixing performance of a wide angle Y-mixer was studied to see whether this is possible. An analysis of characteristic mixing times as a function of the average energy dissipation rate showed that turbulent dispersion of the feed streams determined the rate of the mixing process. The characteristic time for turbulent dispersion was of the same order as an arbitrarily set residence time in the Y-mixer. However, CFD simulations of the flow showed large variation in the spatial distribution of the dissipation rate and revealed unsatisfying macromixing.

1 Introduction

Polymorphism is of great interest to industry because the polymorphs have different physical properties influencing their performance, e.g., the color of pigments and the solubility of pharmaceuticals. Control over the formation is desired. From the viewpoint of thermodynamics only one polymorph is stable. However, in precipitation the formation of less stable polymorphs may be kinetically favored, according to Ostwald's rule of stages. If the nucleation rates and growth rates are in the same range, and transition is slow, concomitant polymorphs will be observed [1].

In precipitation research nucleation rates are generally measured according to the method developed by Nielsen [2,3] for barium sulfate. Two flows of reactant solutions are intensively mixed in a mixing tee and nuclei form in the outlet tube. From crystal size distribution (CSD) data of samples from the resulting suspension the nucleation rate is calculated. Angerhöfer [4] and Schubert [5] applied this method for barium sulfate and Ståhl [6] for benzoic acid. Haselhuhn [7] used the Nielsen method to study the formation of pseudo-polymorphs of calcium oxalate hydrates as a function of supersaturation. Mahajan [8] modified the Nielsen method by varying the residence time in a tube with variable length. The shift in the CSD with residence time was measured and used to calculate nucleation and growth rates for the amino acid asparagine and a drug lovostatine.

In these investigations it was assumed that complete mixing of the reactants preceded nucleation and thus that nucleation took place at a constant supersaturation level. However, recent papers indicate that for some compounds this assumption does not hold: precipitation starts before mixing is still completed. This is especially the case for insoluble compounds, precipitating at high supersaturation levels. Schwarzer [9] and Baldyga [10] precipitated barium sulfate and observed a decrease of the average particle size with increasing mixing intensity indicating the interaction between mixing and nucleation kinetics.

It is the objective of this research program at the Delft University of Technology to measure the competitive nucleation rates of concomitant polymorphs. Mixing of the reactants is crucial to these measurements because the mixing intensity determines the local supersaturation level. A constant supersaturation level must be achieved before nucleation starts. Therefore, this paper presents an assessment of mixing in a typical experimental set-up used to determine nucleation kinetics.

2 Nucleation Theory

The nucleation rate J is represented by the following equation according to the classical nucleation theory[1)]:

$$J = A\exp\frac{-4\Gamma^3}{27\ln^2 S} \quad \text{with} \quad \Gamma = \frac{\nu_m^{2/3}}{k_B T}\left(\sum_i^{hkl} c_i\gamma_i\right) \tag{1}$$

In this equation A is a kinetic parameter and S is supersaturation defined as the ratio of the actual concentration of the compound over its solubility. Ter Horst [11] defines Γ as the dimensionless overall interfacial energy. It contains all unknown parameters γ_i and c_i for all hkl crystal surfaces with γ_i the interfacial energy and c_i a geometrical factor reflecting the surface area. This Γ, rather than its individual parameters, is of great importance in nucleation processes.

Primary nucleation proceeds as a strongly non-linear function of the supersaturation and therefore fluctuations in the supersaturation level due to mixing have a strong effect on the nucleation rate. Polymorphs will be formed at different rates because all three parameters A, Γ and S in equation (1) may be different. Polymorphs experience different super-

[*] Prof. dr ir P. J. Jansens, dr ir H.J.M. Kramer, dr ir J. H. ter Horst and ir C. P. M. Roelands (author to whom correspondence should be addressed, e-mail: m.roelands@wbmt.tudelft.nl), Laboratory for Process Equipment, Delft University of Technology, Leeghwaterstraat 44, 2628CA, Delft, The Netherlands; Dr ir J. J. Derksen: Kramers Laboratorium voor Fysische Technologie, Delft University of Technology, Prins Bernhardlaan 6, 2628BW, Delft, The Netherlands.

1) List of symbols at the end of the paper.

  0930-7516/03/0303-0296 $ 17.50+.50/0

saturation levels at a certain concentration level $c_0 > c^{II}_{eq}$ because the solubility c^{I}_{eq} of the stable polymorph is always lower than the solubility c^{II}_{eq} of the less stable polymorph. Concentration fluctuations may therefore affect the polymorph composition of the precipitate by promoting the formation of either one of the polymorphs.

To measure the nucleation rate of the polymorphs at a fixed composition according to the method described in the introduction, the nucleation process has to take place at a constant value for the supersaturation level. Therefore, mixing should be completed down to molecular scale before nuclei form.

3 Time Scale Analysis

3.1 Experimental Setup

Time scale analysis is done for a typical experimental set-up to measure nucleation rates in a precipitation process, shown in Fig. 1. The flows are generated using low-pulse gear pumps. Main components are the wide angle Y-mixer and the precipitation tube. The inner diameter of the tubing D is

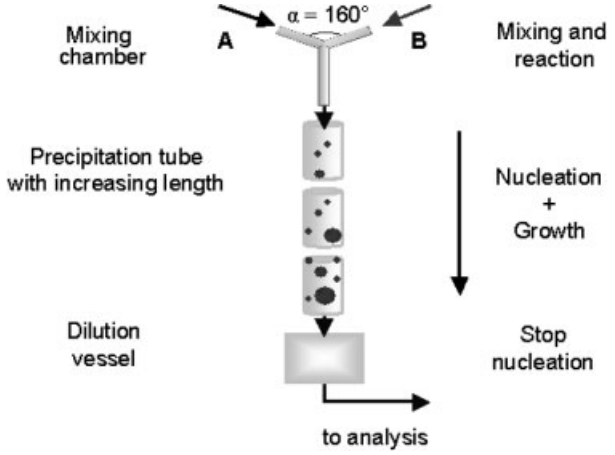

Figure 1. Experimental setup with the wide angle Y-mixer.

$3 \cdot 10^{-3}$ m. The length of the precipitation tube can be varied from 1 to 2 and to 6 m. The average flow velocity U in the outlet tube is 6 m s^{-1} corresponding to a Reynolds number of $1.8 \cdot 10^4$, with $\mathrm{Re} = UD/\nu$ and kinematic viscosity $\nu = 1 \cdot 10^{-6}$ m^2 s^{-1} for water. Under these plug-flow conditions a narrow residence time distribution is expected. At the end of the tube the suspension is quenched into a vessel filled with saturated solution to inhibit further nucleation. From this vessel samples will be collected to determine the crystal size distribution and the polymorph composition.

3.2 Mixing Time Scales

Nucleation rate measurements at high supersaturation level will be carried out in the wide angle Y-mixer. In this geometry rapid mixing down to molecular scale has to be achieved before nuclei form. However, it is not possible to set this minimum for the mixing time, as the nucleation time is unknown. Direct observation of the nucleation time is not possible due to the small size of the nuclei and the statistical character of the nucleation process. Therefore, in this study the required time for complete mixing is arbitrarily set as the residence time of the reacting mixture flowing through the outlet tube over a length of twelve times its diameter:

$$\tau_r = \frac{12D}{U} \tag{2}$$

Initially, in the Y-mixer the opposing reactant flows are completely segregated. Upon impact of the flows the reactants are first dispersed by large eddies then transported by cascading eddies that decay finally towards the scale for molecular diffusion. The time scales that are characteristic for these mixing processes were estimated according to the mechanistic model by Baldyga [12].

Mixing times are written down as a function of the dissipation rate of the turbulent kinetic energy ε. The mean dissipation rate of the turbulent kinetic energy is calculated from an estimate of the pressure drop over the outlet tube of the Y-mixer according to

$$\varepsilon = \frac{\phi_v \Delta P}{\rho V} = \frac{2fU^3}{D} \quad \text{with} \quad 4f = 0.316\mathrm{Re}^{-0.25} \tag{3}$$

In this equation ϕ_v is the flow rate, V the volume of the outlet tube and f the friction factor for the tube wall. Under the conditions described above, the mean dissipation rate in the tube ε is of the order of $1 \cdot 10^3$ m^2 s^{-3}.

It must be noted that the pressure drop is calculated for well-developed turbulent flow in the outlet tube. The pressure drop over the actual Y-mixer is expected to be larger and therefore the local energy dissipation rate may be higher. Measurement of the pressure drop over the Y-mixer would improve the estimate of the mean dissipation rate.

First there is the time scale τ_D for turbulent dispersion or macromixing. This time scale takes into account the large-scale mass transfer of the reactants across the turbulent flow, but not molecular diffusion [13].

$$\tau_D = \frac{L_0^2}{D_T} \tag{4}$$

In this equation L_0 is the characteristic dimension of the system, set at half the tube diameter. For the Y-mixer this scale is equal to the length scale of initial segregation. D_T represents turbulent diffusivity, estimated from $D_T = \nu_t / Sc_T$ with turbulent viscosity $\nu_t = C_\mu k^2/\varepsilon$ with constants $Sc_T = 0.7$ and $C_\mu = 0.09$ [12]. The turbulent kinetic energy $k = 3/2u'^2$ with $u' \approx 1.1$ m s^{-1} the root mean square of the velocity fluctuation estimated from $\varepsilon = u'^3/L_0$.

Next, there is the time-scale for the disintegration of large eddies to smaller eddies, reducing the size of concentration fluctuations (inertial-convective mixing) [12]:

$$\tau_s = \frac{3}{4} \frac{L^{2/3}}{\varepsilon^{1/3}} \tag{5}$$

With L the scale of large energy containing eddies being equal to the initial segregation scale for the Y-mixer.

The final size of these eddies is characterized by the Kolmogorov length $\eta_k = (\nu^3/\varepsilon)^{1/4}$. In this case the Kolmogorov length $\eta_k \approx 6 \cdot 10^{-6}$ m. By the process of viscous-convective mixing these eddies decay and the scale for concentration fluctuations goes from the Kolmogorov scale towards the scale for diffusion or Batchelor scale. This processes is characterized by the engulfment rate E (viscous-convective mixing) [12]:

$$\tau_E = \frac{1}{E} = 17.24\left(\frac{\nu}{\varepsilon}\right)^{1/2} \quad (6)$$

The Batchelor scale $\eta_B = \eta_k\, Sc^{-1/2}$ with the Schmidt number $Sc = \nu/D_m$, the ratio of the kinematic viscosity over the molecular diffusion coefficient $D_m \approx 1 \cdot 10^{-9}\,\mathrm{m^2\,s^{-1}}$. For low concentrated aqueous solutions the Schmidt number is approximately $1 \cdot 10^3$ so the Batchelor scale for molecular diffusion is about 30 times smaller ($\eta_B \approx 2 \cdot 10^{-7}$ m) than the Kolmogorov length scale.

Finally, diffusion of the reactant solutions into each other takes place over the Batchelor length scale (viscous-diffusive mixing):

$$\tau_{diff} = \frac{\eta_B^2}{D_m} \quad (7)$$

Tab. 1 shows the calculated characteristic mixing times scaled over the average residence time in the outlet tube over a length of twelve diameters.

Table 1. Dimensionless mixing time scales.

τ_D / τ_r	τ_s / τ_r	τ_E / τ_r	τ_{diff} / τ_r
0.78	0.17	0.09	0.01

It can be observed that the characteristic time τ_D for turbulent dispersion is comparable to the average residence time. The eddy-disintegration time τ_s and the engulfment time τ_E are one order of magnitude smaller and the time for diffusion τ_{diff} is two orders smaller. This analysis reveals that turbulent dispersion is the rate-determining step for mixing the flows down to the molecular level.

The mechanistic approach to calculate characteristic mixing times requires an average value for the energy dissipation rate. This value was estimated by considering the flow in the outlet tube as a well-developed turbulent flow. However, the flow pattern in the wide angle Y-mixer, with two jets colliding, is likely to be different. Within the Y-mixer large differences in the distribution of energy dissipation rates are expected. In the following section a method based on computational fluid dynamics is described to estimate characteristic mixing times taking into account these differences.

4 Computational Fluid Dynamics Simulations

4.1 CFD Setup

The flow in the wide angle Y-mixer was simulated with Computational Fluid Dynamics (CFD) using Fluent 6.0.20 software. For the simulations the physical properties of water were used at a pressure of 1 bar and temperature of 300 K. The flow in a wide angle Y-mixer was simulated with three circular channels all having the same diameter of $3 \cdot 10^{-3}$ m. The length of the inlet tubes was $25 \cdot 10^{-3}$ m and the length of the outlet tubes was $35 \cdot 10^{-3}$ m. The angle between the inlet channels was 160°. The average velocity of the flow was 3 m s^{-1} in the two inlet tubes and 6 m s^{-1} in the outlet tube, corresponding with a Reynolds number of $9 \cdot 10^3$ in the inlet tube and $18 \cdot 10^3$ in the outlet tube.

A 3D grid consisting of $144 \cdot 10^3$ cells was defined using Gambit 2.0.4 software representing half the volume of the Y-mixer making use of the symmetry plane dividing all channels in half. The first four cells near the wall with a total thickness of $0.23 \cdot 10^{-3}$ m or 15 % of the inner radius were used to represent the boundary layer.

For closure of the Reynolds Averaged Navier-Stokes equations the k-ε model was used. This model assumes isotropic turbulence. The flow near the wall was described by wall functions and adjacent to the wall by the laminar stress-strain relationship. As boundary conditions for the inlet user defined profiles for the velocity, kinetic energy and dissipation were applied. The outlet boundary condition was set as zero gradient.

Macromixing of two non-reacting species A and B by convection and by turbulent diffusion was simulated. The mass fractions of A and B were set at 0.1 for each inlet. Molecular diffusion coefficients for A and B were set at $10^{-9}\,\mathrm{m^2\,s^{-1}}$. No sub-grid scale model was applied to take into account micromixing within the grid cells. This implies that if in a grid cell both species are present, they are completely mixed.

4.2 Macromixing and Dissipation Rate

The pattern of two impacting flows in the wide angle Y-mixer was expected to result in a distribution of energy dissipations rates and therefore in different mixing times. In Fig. 2 velocity vectors are shown for the center plane through the Y-mixer. The vectors have a length proportional to the velocity at the point of origin of the vector. High velocities can be observed at the edges of the outlet tube. Directly behind the edges, near the wall, a recirculating flow can be observed. An almost stagnant zone is visible in the top of the Y-mixer. Not all vectors are shown here to enable interpretation of the figure.

In Fig. 3 the contour plot of mass fraction A and B is shown and the wedge-shaped macromixed zone where the species mix can be observed. Directly behind the edges near the wall of the outlet tube the flow is still completely unmixed at

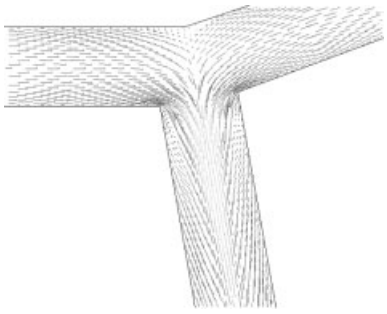

Figure 2. Velocity vector plot for the center plane through the wide angle Y-mixer.

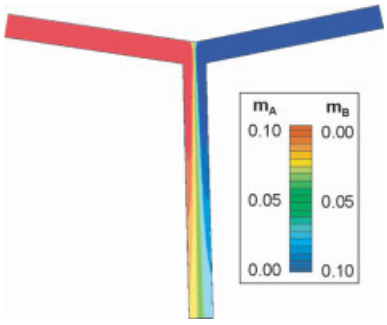

Figure 3. Contour plot of the mass fraction of species A and B.

macro-level and remains so over a length of several pipe diameters.

Fig. 4 is a contour plot of the rate of dissipation of turbulent kinetic energy in the center plane of the Y-mixer. It shows that a large variation in levels of the dissipation rate exists at the edges between the inlet tubes pipes with the outlet tube. From Fig. 3 it can be observed that in these zones the flows are unmixed at macro scale so the high-energy dissipation rate is not effectively used in these zones for mixing. In the plane where the two flows collide high-energy dissipation rates occur as well, but here they coexist with a zone that is, at least at macro scale, well mixed.

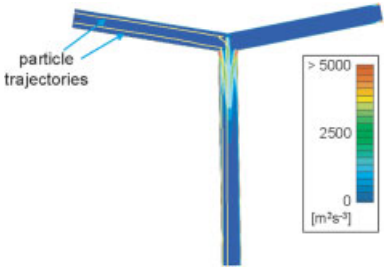

Figure 4. Contour plot of the turbulent kinetic energy dissipation rate ε with particle trajectories for two particles.

4.3 Mixing Times from Particle Tracking

Particle tracking is used as a computational method to investigate macromixing flow patterns. Inert particles were defined to resemble fluid elements and have no influence on the flow. The trajectories of the fluid elements were followed during their movement with the average flow. Each trajectory was calculated by stepwise integration over discrete time steps. The effect of turbulent velocity fluctuations on the course of the fluid elements was not taken into account.

On their way through the Y-mixer the fluid elements encounter zones with different levels of turbulent energy dissipation and with different concentrations of the species A and B. A total number of 254 fluid elements were followed with their starting positions equally distributed over the inlet plane.

Trajectories for some fluid elements are shown in Fig. 4. For two fluid elements the levels of the energy dissipation rate and of the dimensionless product of the mass fractions of A and B are shown in Fig. 5. The mass fraction product was made dimensionless by dividing it by the product of its mean concentrations in the outlet tube. In these figures a value of 0 for this product means that only one of the species is present, a value of 1 means that both species are present in equal amounts. The mass fraction product is considered here as a measure for macromixing and the energy dissipation rate for micromixing.

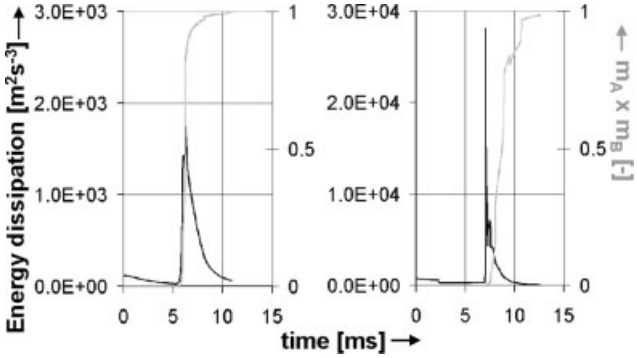

Figure 5. Plots of the energy dissipation rate (black line) and mass fraction product (gray line) encountered by two particles on their way through the wide angle Y-mixer.

The maximum level of energy dissipation experienced by the fluid elements during their way through the wide angle Y-mixer differs up to one order in magnitude, as can be seen in Fig. 5. For the fluid element on the left side, the zone of high-energy dissipation coincides with the zone with a high dimensionless mass fraction product. It is expected that in this zone the reactants mix effectively down to the molecular level.

The fluid element on the right side of Fig. 5 moves first through a zone with a very high rate of energy dissipation. However, in this zone the high energy dissipation rate does not contribute to the mixing because the mass fraction product remains zero, meaning that at macro-level the fluid element is still unmixed.

The contour plots of the distribution of species A an B were used to define a 'residence time for effective macromixing' t_{rm} for the fluid elements on their way through the mixing geometry. The starting point for this time period is the point

where the dimensionless mass fraction product exceeds an arbitrarily set value of $1 \cdot 10^{-8}$. Such a value may be used in future to define the supersaturation level. This period ends when a fluid element has left the simulated grid. It is stressed that at the endpoint of the grid mixing of the flows is not necessarily completed. In Fig. 6 these times are shown as a function of the starting positions of the fluid elements in the inlet plane.

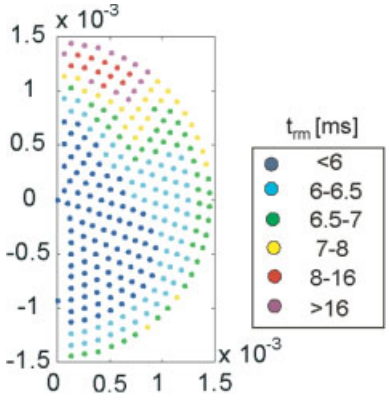

Figure 6. Distribution of residence times for macromixing of the fluid elements as function of starting position.

The fluid elements starting near the wall have slightly longer residence times than those starting in the center. This is to be expected as the fluid elements follow the average flow velocities that are a bit lower near the wall compared to those in the center. Remarkable is that the macromixing residence times for the elements released in the top zone of the tube are about 2–3 times longer than those for elements in the rest of the tube. Their path through the stagnant top-zone of the Y-mixer causes these longer residence times. For our purpose of premixing two feed streams in this geometry before nucleation can take place, these fluid elements are to be considered with caution. If micromixing proceeds within this time period as well, undesired nuclei formation may take place in these elements before the bulk of the flow is mixed.

For the fluid elements the level of the energy dissipation rate can be followed over the residence time for effective macromixing. This was done for two characteristic time scales for mixing: the time scale for turbulent dispersion and for engulfment. For each fluid element these time scales, being functions of the local energy dissipation rate, were averaged over the residence time according to the flowing equation:

$$\overline{\tau}_m = \frac{\int_0^{t_{rm}} \tau_m(\varepsilon)\,dt}{t_{rm}} \tag{8}$$

In Figs. 7 and 8 the averaged time scales for turbulent dispersion and for engulfment for the 254 fluid elements are shown versus the macromixing residence time t_{rm}. At the diagonal line the averaged mixing times and the residence times are equal. In this figure it can be observed that most of the fluid elements have residence times around 7 milliseconds,

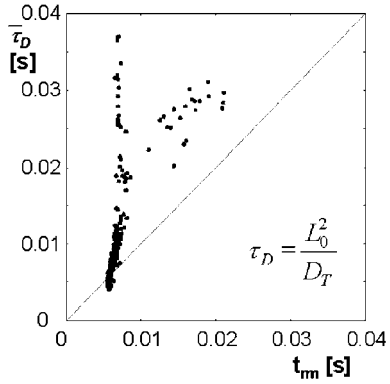

Figure 7. Averaged turbulent dispersion time as function of the macromixing residence time for 254 fluid elements.

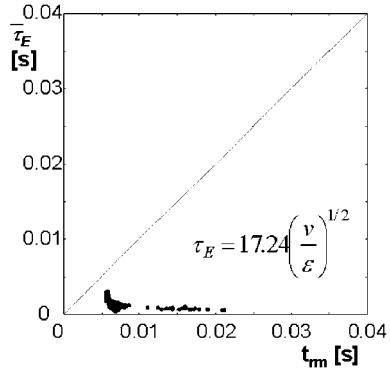

Figure 8. Averaged time for engulfment as function of the macromixing residence time for 254 fluid elements.

except the fluid elements caught in the top zone of the Y-mixer which have residence times 2–3 times longer.

Most of the points in Fig. 7 lie above the diagonal line, with the averaged turbulent dispersion times being longer than the residence times. This means that most of the fluid elements are not mixed at macroscale when they leave the outlet tube after a length of twelve diameters. This agrees with the contour plots of the mass fractions of the species A and B observed in Fig. 3.

In Fig. 8 for all points that lie below the diagonal line, the averaged characteristic time for engulfment (micromixing) is smaller than the residence time. This means that mixing at micro scale is not limiting the overall mixing process over the reference length of the outlet tube of twelve diameters.

4.4 Some Remarks on the CFD Simulations

In this study time-averaged flow simulations were carried out instead of time-dependent simulations because the flow in the wide angle Y-mixer is likely to be steady in time, e.g., non-oscillating. The k-ε turbulence model was selected assuming isotropic turbulence. The Reynolds Stress Model may be selected for flows with anisotropic turbulence, for example swirling flows.

The flow in the boundary layer was described by semi-empirical formulas or wall functions. The alternative to this approach is to resolve the flow in the near wall region down to the wall with modified turbulence models valid in this region and a sufficiently fine grid at the cost of increased computational resources.

Mixing of the non-reacting species A and B was followed at macro level. A typical grid cell is much larger than the length scales for micromixing with a cell dimension of $60 \cdot 10^{-6}$ m while typical Kolmogorov and Batchelor length scales are $6 \cdot 10^{-6}$ m and $0.2 \cdot 10^{-6}$ m respectively. To include micromixing within the grid cells a micromixing model should be introduced.

Particle tracking was carried out for fluid elements that followed trajectories calculated from average flow velocities. The random effect on the path of turbulent velocity fluctuations was not taken into account. Under the assumption that these are up to 15 % of the mean velocity, they may have a significant effect on the trajectories. To include the effect of the velocity fluctuations an approach similar to that of Rielly [14] may be followed.

In future work it is tempting to study the effect on macromixing of an alternative turbulence model, of different boundary conditions and of velocity fluctuations on the track of fluid elements. Validation of the CFD simulations may be achieved by comparing the calculated pressure drop with experimental values.

Another way to make the mixing process more efficient is to enlarge the zones where both species are present in combination with a high energy dissipation rate (e.g. the collision plane) while reducing the zones that have high energy dissipation rate but lack either one of the species (downstream the edges between inlet and outlet tubes). This may be achieved by decreasing the angle between the inlet tubes. This may also reduce the stagnant zone in the top of the wide angle Y-mixer. The angle should not be too narrow because the flows should still collide with sufficient impact. The Roughton mixer can be considered as an extreme case of such a mixing device. In this geometry the inlets are mixed with a swirling flow while edges near wall (and stagnant zones) have disappeared. Both alternative geometries are shown in Fig. 9. These options support the need for additional simulations in combination with experimental validation by comparison with the measured pressure drop over the Y-mixer.

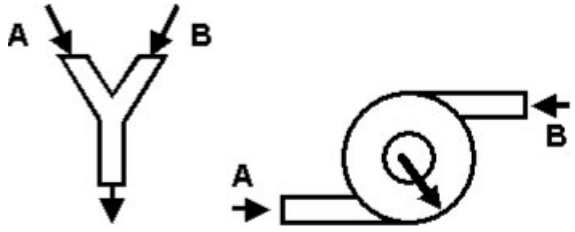

Figure 9. Alternative mixers: narrow angle Y-mixer and Roughton mixer.

5 Discussion

To measure nucleation rates of concomitant polymorphs complete mixing of the reactants creating supersaturation is desired before nucleation starts. The question is whether or not the wide angle Y-mixer is suitable for this purpose. The time scales from section 3, based on an estimate of the average dissipation rate, do not correspond with the averaged time scale distributions from section 4. From time scale analysis one may conclude that the geometry is suitable, with macromixing being the limiting step. From the CFD simulation however, it follows that macromixing is not completed over a length of the outlet tube of twelve diameters (corresponding with a residence time of approximately $6 \cdot 10^{-3}$ s). Although very high energy dissipation rates are achieved in this Y-mixer, fluid elements moving through this geometry only experience these high rates during very short times and partially also in zones where only one of the species is present.

To improve mixing a few options exist. First, to enhance macromixing in the outlet tube a static mixer can be inserted. This is, however, a costly improvement because the pressure drop over the wide angle Y-mixer is expected to increase approximately 100 times. Furthermore, there may be small stagnant zones in a static mixer, giving rise to long residence times for fluid where undesired nucleation may occur.

The effect of mixing rate on the average size of precipitates was observed experimentally by Schwarzer [9] and by Baldyga [10] for barium sulfate and by Manth [15] for strontium sulfate. By increasing the Reynolds number to a sufficiently large value the CSD does not change anymore. It may be concluded that up from these values the effect of mixing on the formation of the crystals has disappeared. It is not clear yet whether the increase of the mixing intensity results in complete premixing of the reactants before nuclei form or that some kind of mixing limitation was overcome. These experiments were done with insoluble, rapidly precipitating inorganic compounds. Nucleation may start at the interface between fluid elements of the reacting species before these are completely mixed.

Rieger [16] analyzed precipitates of Boehmite and an organic pigment shortly after mixing. Cryo-TEM images showed two-phase liquid regions shortly ($1 \cdot 10^{-2}$ s) after mixing. The authors found that nucleation had taken place at the interface between the regions. If this behavior applies to all precipitates, the method proposed in this paper to separate in time and place the creation of supersaturation (chemical reaction) from nucleation (physical reaction) may be not possible. However, this phenomenon may be limited to very rapidly precipitating (very insoluble) compounds. In-line measurement of the composition of reaction mixtures and of the processes taking place directly after mixing the reactants may give more answers.

6 Conclusions

The measurement of nucleation rates of concomitant polymorphs requires that complete mixing precedes nucleation. This means that the time scale for mixing must be smaller than the time scale for nucleation. Two analyses were performed to verify whether this condition was met in a wide angle Y-mixer. First mixing time scales were estimated as a function of the average dissipation rate of turbulent kinetic energy. These times were compared to the residence time for the flow through the outlet tube. The time for turbulent dispersion (macromixing) was the rate-determining step being of the same order as the residence time. Therefore, mixing was complete over a length of the outflow tube equal to twelve times its diameter.

However, CFD simulations of the mixing process in the wide angle Y-mixer revealed large spatial differences in energy dissipation rate. There were zones observed with high energy dissipation rates where no mixing occurred because either one of the species was lacking. By means of particle tracking two averaged characteristic mixing times were calculated and compared to effective residence times for macromixing. From the simulations it followed that turbulent dispersion was not complete at the end of the outlet tube. Macromixing may be improved by introducing a static mixer in this tube.

Acknowledgement

The authors wish to thank Aimée Tan for her contribution and are grateful to Akzo Nobel, BASF, Bayer and DSM for their support. This project is part of the M3 program of the Delft University of Technology.

Received: December 19, 2002 [CET 1790]

Symbols used

A	[m^{-3} s^{-1}]	pre-exponential kinetic parameter
c_i	[–]	geometrical factor for surface area
c_{eq}	[moles kg^{-1}]	solubility per kg solvent
D	[m]	tube diameter
D_m	[m^2 s^{-1}]	molecular diffusion coefficient
D_T	[m^2 s^{-1}]	turbulent diffusion coefficient
E	[s^{-1}]	engulfment rate
f	[–]	friction factor
G	[m s^{-1}]	growth rate
J	[m^{-3} s^{-1}]	nucleation rate
k	[m^2 s^{-2}]	turbulent kinetic energy
k_B	[J K^{-1}]	Boltzmann constant
L_0	[m]	initial length scale for turbulence
P	[N m^{-2}]	pressure
Re	[–]	Reynolds number
S	[–]	supersaturation
Sc	[–]	Schmidt number
Sc_T	[–]	turbulent Schmidt number
T	[K]	temperature
t_{rm}	[s]	residence time for effective macromixing
u	[m s^{-1}]	average flow velocity
u'	[m s^{-1}]	mean root square of the turbulent velocity fluctuation
V	[m^3]	volume
Γ	[–]	dimensionless overall interfacial energy
γ_i	[N m^{-2}]	interfacial energy
ε	[m^2 s^{-3}]	energy dissipation rate [W kg^{-1}]
ϕ_v	[m^3 s^{-1}]	flow rate
η_B	[m]	Batchelor length scale
η_k	[m]	Kolmogorov length scale
ν	[m^2 s^{-1}]	kinematic viscosity
ν_m	[m^3]	molecular volume
ν_T	[m^2 s^{-1}]	turbulent viscosity
ρ	[kg m^{-3}]	density
τ_D	[s]	time scale for turbulent dispersion
τ_{diff}	[s]	time scale for molecular diffusion
τ_E	[s]	time scale for engulfment
τ_r	[s]	mean residence time
τ_s	[s]	time scale for disintegration of large eddies

References

[1] J. Bernstein, R. J. Davey, J. O. Henck, *Angew. Chem. Int. Ed.* **1999**, *38*, 3440.
[2] A. E. Nielsen, *Acta Chem. Scand.* **1961**, *15*, 441.
[3] A. E. Nielsen, *Kinetics of Precipitation*, Pergamon, Oxford **1964**.
[4] M. Angerhoefer, *Ph.D. Thesis*, TU Muenchen **1994**.
[5] H. Schubert, A. Mersmann, *Trans IChemE* **1996,** *74A*, 821.
[6] M. Ståhl, B.L. Åslund, Å C. Rasmuson, *AIChE J.* **2001**, *47*, 1544.
[7] F. Haselhuhn, M. Kind, in *Proc. of the 15th Int. Symp. on Ind. Cryst.* (Ed: A. Chianese), AIDIC, Milano **2002**.
[8] A. M. Mahajan, D. J. Kirwan, *J. Cryst. Growth* **1994**, *144*, 281.
[9] H. C. Schwarzer, W. Peukert, *Chem. Eng. Technol.* **2002**, *25*, 657.
[10] J. Baldyga,W. Orchiuch, *Chem. Eng. Sci.* **2001**, *56*, 2435.
[11] J. H. Ter Horst, H. J. M. Kramer, P. J. Jansens, *Cryst. Growth Des.* **2002**, *2*, 351.
[12] J. Baldyga, J. R. Bourne, *Turbulent Mixing and Chemical Reactions*, Wiley, Chichester **1999**.
[13] B. Yu. Shekunov, J. Baldyga, P. York, *Chem. Eng. Sci.* **2001**, *56*, 2421.
[14] C. D. Rielly, A. J. Marquis, *Chem. Eng. Sci.* **2001**, *56*, 2475.
[15] Th. Manth, D. Mignon, H. Offermann, *Chem. Eng. Sci.* **1996**, *51*, 2571.
[16] J. Rieger, D. Franke, T. Frechen, H. Haberkorn, W. Goesele, in *Proc. of the 9th Int. Workshop. on Ind. Cryst.(BIWIC)* (Ed: J. Ulrich), Halle **2002**.

